Title

Three-dimensional modeling of outcrop-to-outcrop hydrothermal circulation on the eastern flank of the Juan de Fuca Ridge

Journal

Journal of Geophysical Research: Solid Earth, 121(3)

ISSN

2169-9313

Authors

Winslow, DM
Fisher, AT
Stauffer, PH
et al.

Publication Date

2016-03-01

DOI

10.1002/2015jb012606

Peer reviewed

AGU PUBLICATIONS

JGR

Journal of Geophysical Research: Solid Earth

RESEARCH ARTICLE
10.1002/2015JB012606

Key Points:
- Outcrop-to-outcrop hydrothermal simulations elucidate hydrologic properties and flow characteristics
- Three-dimensional simulations make significant gains over work in two dimensions
- Additional outcrops increase overall recharge rates and reduce outflow at the primary discharge site

Supporting Information:
- Letter S1
- Texts S1 and S2 and Figures S1 and S2

Correspondence to:
A. T. Fisher,
afisher@ucsc.edu

Citation:
Winslow, D. M., A. T. Fisher, P. H. Stauffer, C. W. Gable, and G. A. Zyvoloski (2016), Three-dimensional modeling of outcrop-to-outcrop hydrothermal circulation on the eastern flank of the Juan de Fuca Ridge, *J. Geophys. Res. Solid Earth*, *121*, doi:10.1002/2015JB012606.

Received 17 OCT 2015
Accepted 19 FEB 2016
Accepted article online 22 FEB 2016

Three-dimensional modeling of outcrop-to-outcrop hydrothermal circulation on the eastern flank of the Juan de Fuca Ridge

D. M. Winslow[1], A. T. Fisher[1], P. H. Stauffer[2], C. W. Gable[2], and G. A. Zyvoloski[2]

[1]Earth and Planetary Sciences Department, University of California, Santa Cruz, California, USA, [2]Earth and Environmental Sciences Division, Los Alamos National Laboratory, Los Alamos, New Mexico, USA

Abstract We present three-dimensional simulations of coupled fluid and heat transport in the ocean crust, to explore patterns and controls on ridge-flank hydrothermal circulation on the eastern flank of the Juan de Fuca Ridge. Field studies have shown that there is large-scale fluid flow in the volcanic ocean crust in this region, including local convection and circulation between two basement outcrops separated by ~50 km. New simulations include an assessment of crustal permeability and aquifer thickness, outcrop permeability, the potential influence of multiple discharging outcrops, and a comparison between two-dimensional (profile) and three-dimensional representations of the natural system. Field observations that help to constrain new simulations include a modest range of flow rates between recharging and discharging outcrops, secondary convection adjacent to the recharging outcrop, crustal permeability determinations made in boreholes, and the lack of a regional seafloor heat flux anomaly as a consequence of advective heat loss from the crust. Three-dimensional simulations are most consistent with field observations when models use a crustal permeability of 3×10^{-13} to 2×10^{-12} m^2, and the crustal aquifer is $\leq$300 m thick, values consistent with borehole observations. We find fluid flow rates and crustal cooling efficiencies that are an order of magnitude greater in three-dimensional simulations than in two-dimensional simulations using equivalent properties. Simulations including discharge from an additional outcrop can also replicate field observations but tend to increase the overall rate of recharge and reduce the flow rate at the primary discharge site.

1. Introduction

1.1. Background and Motivation

Ridge-flank hydrothermal systems drive substantial flows through the oceanic crust on a global basis. These systems, which operate at lower temperatures and in older ocean crust than that found near ridges, extend over a large fraction of the seafloor. In aggregate, ridge-flank systems are responsible for $\geq$70% of advective heat extraction from the oceanic crust, equivalent to 4–7 TW [*Stein and Stein*, 1992, 1994; *Hasterok*, 2013b], and mediate significant solute fluxes between the crust and the ocean [*de Villiers and Nelson*, 1999; *Wheat and Mottl*, 2004; *Fisher and Wheat*, 2010]. These flows also influence the physical and chemical evolution of the crust [*Alt*, 2004; *Bartetzko*, 2005] and support a vast and diverse biosphere within the sediments and upper volcanic crust [*Cowen et al.*, 2003; *Edwards et al.*, 2005].

Much of the ridge-flank environment is covered by thick and relatively impermeable sediment [*Spinelli et al.*, 2004]. Seamounts and volcanic edifices (outcrops) exposed at the seafloor can allow fluids to bypass sediments, providing relatively high-permeability conduits for fluid exchange between the ocean and underlying crustal aquifer [*Villinger et al.*, 2002; *Fisher et al.*, 2003b; *Fisher and Wheat*, 2010]. Systems that develop sustained subsurface flow between sets of outcrops are referred to as outcrop-to-outcrop hydrothermal siphons and are capable of driving fluids through the ocean crust at rates that measurably impact lithospheric heat extraction if crustal and outcrop permeability are sufficiently high [*Fisher et al.*, 2003a; *Hutnak et al.*, 2008; *Anderson et al.*, 2012]. This type of flow is driven by differences in pressure between cool (recharging) and warm (discharging) columns of water within each outcrop [*Fisher and Becker*, 2000; *Fisher et al.*, 2003b; *Winslow and Fisher*, 2015].

Volcanic rock outcrops are ubiquitous throughout the seafloor [*Kim and Wessel*, 2011], including exposures found in fracture zones, transform faults, and other sites of basement exposure. Given the global number of outcrops, the typical spacing between pairs of these features should allow for many hydrothermal siphons to operate [*Anderson et al.*, 2012]. These systems may be more important for lithospheric heat extraction than

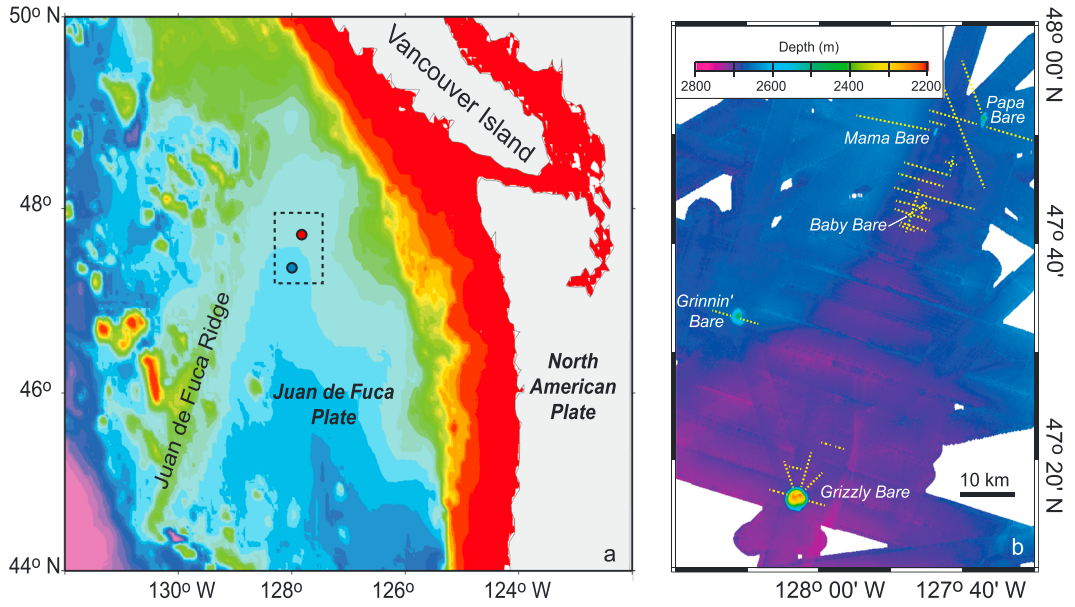

Figure 1. Map of field site. (a) Location of field site on eastern flank of the Juan de Fuca Ridge. Blue and red dots depict locations of the Grizzly Bare and Baby Bare outcrops, respectively. Dashed box shows location of Figure 1b. (b) Bathymetry and locations of volcanic rock outcrops seafloor heat flux measurement transects [*Hutnak et al.*, 2006].

previously estimated because small outcrops, which are underrepresented in gravity studies and rarely mapped [*Kim and Wessel*, 2011], tend to be sites of discharge [*Fisher et al.*, 2003b; *Davis and Becker*, 2004; *Hutnak et al.*, 2008; *Winslow and Fisher*, 2015].

In this study, we focus on a well-studied outcrop-to-outcrop hydrothermal siphon operating on the eastern flank of the Juan de Fuca Ridge. We present a series of coupled-flow simulations designed to elucidate the nature of heat and fluid flow within this field area and to constrain hydrologic properties using field observations. Most new simulations are completed using a three-dimensional geometry, but a subset of simulations are completed in two dimensions, following an approach that has been applied to systems of this kind in the past [*Stein and Fisher*, 2003; *Hutnak et al.*, 2006]. We also assess the potential for a secondary discharging outcrop to influence patterns of heat and fluid flow within the ocean crust in this setting.

1.2. Field Site and Observations

1.2.1. Characterization of Field Site

The field area that is the basis for modeling is located on ~2 to 5 Myr old seafloor, 60 to 140 km east of the Juan de Fuca Ridge, an intermediate rate spreading center (Figure 1). Despite being relatively young, a thick layer of turbidites and hemipelagic sediment has accumulated (up to 900 m) above much of the volcanic ocean crust in this region due to high sedimentation rates and the trapping of sediment by abyssal hill topography [*Davis et al.*, 1992, 1999; *Underwood et al.*, 2005]. Volcanic outcrops penetrate the otherwise thick and continuous sediments in a few locations, providing pathways for fluids to enter and exit the crustal aquifer [*Davis et al.*, 1992]. Two volcanic outcrops, Grizzly Bare and Baby Bare, comprise entry and exit sites for an active hydrothermal siphon that drives fluids from south to north across ~50 km of crust [*Wheat et al.*, 2000; *Fisher et al.*, 2003b; *Hutnak et al.*, 2006; *Winslow and Fisher*, 2015]. These outcrops are located on ~3.5 Myr old seafloor and were most likely formed by off-axis volcanism, through processes distinct from those governing the initial formation of the crust [*Karsten et al.*, 1998; *Becker et al.*, 2000]; for this reason, hydrologic properties within each outcrop may differ from those of the nearby and underlying basaltic crust. There are additional basement outcrops on this part of the ridge flank (Figure 1), including Mama Bare (16 km to the north of Baby Bare, along the trend of a buried basement ridge) Papa Bare (20 km to the northeast), and Zona Bare (34 km to the north of Mama Bare) [*Davis et al.*, 1992; *Wheat et al.*, 2000; *Hutnak et al.*, 2006].

The crustal aquifer in this region comprises one or more layers of extrusive basalt that extend hundreds of meters beneath the sediments, although the maximum depth of fluid circulation is not well known. In situ bulk permeability measurements at the study site, made with borehole packer tests [*Becker and Fisher*, 2008;

Becker et al., 2013], the cross-hole response to the flow of water into one borehole [*Fisher et al.*, 2008], and modeling of thermal logs in flowing boreholes [*Fisher et al.*, 1997; *Becker and Davis*, 2003; *Winslow et al.*, 2013], indicate values in the upper ~320 m of basaltic crust of 10^{-12} to 10^{-11} m^2. Although no boreholes deeper than ~320 m into the volcanic crust have been drilled in this region, Hole 504B (drilled on medium-spreading rate seafloor south of the Costa Rica Rift) shows a significant decrease in permeability deeper than 600 m below the sediment-basement contact [*Anderson et al.*, 1985; *Becker*, 1989, 1996].

Hydrothermal circulation around the field site is likely to have been more vigorous in the past, but rapid sedimentation has reduced the intensity of ridge-flank hydrothermal activity by burying many former outcrops [*Davis et al.*, 1992; *Hutnak and Fisher*, 2007]. Heat flux surveys run on 3.4 to 3.6 Myr old seafloor near the center of this region indicate a present-day heat flux deficit of ~15%, based on comparison with what is predicted by lithospheric cooling models [e.g., *Parsons and Sclater*, 1977; *Stein and Stein*, 1992; *Hasterok*, 2013a], even after correcting for rapid sedimentation [*Hutnak et al.*, 2006]. This deficit can be accounted for by thermal rebound following the slowing or cessation of advective heat loss from the crust [*Hutnak and Fisher*, 2007], a process that can last millions of years after burial of fluid entry and exit points by low-permeability sediments.

1.2.2. Siphon Observations

The existence of the hydrothermal siphon between Grizzly Bare and Baby Bare outcrops has been demonstrated through multiple lines of evidence. Heat flux measurements close to Grizzly Bare show reduced heat flux and cool upper aquifer temperatures: 80 to 100 mW/m^2 and ~5°C, compared to background values of 175 to 185 mW/m^2 and 60 to 65°C at >1 km from the outcrop edge [*Fisher et al.*, 2003b; *Hutnak et al.*, 2006]. This pattern indicates the flow of cold bottom water into the outcrop. In contrast, seafloor heat flux measured near and across Baby Bare is elevated (>800 mW/m^2 adjacent to the outcrop, >10 W/m^2 on the outcrop), consistent with the rise and subsequent discharge of warm crustal fluids [*Becker et al.*, 2000; *Wheat et al.*, 2004; *Hutnak et al.*, 2006]. Sedimentary pore fluids and spring waters from Baby Bare are geochemically distinct from bottom water samples and consistent with increased alteration and water age [*Mottl et al.*, 1998; *Wheat and Mottl*, 2000], and with the composition of fluid samples collected from nearby boreholes [e.g., *Wheat et al.*, 2003, 2010]. Crustal hydrothermal fluids show a clear pattern of increasing alteration along a south-to-north transect [*Wheat and Mottl*, 2000; *Wheat et al.*, 2000]. Analyses of ^{14}C in upper basement fluids from boreholes and Baby Bare suggests a fluid age of 4 to 10 kyr [*Elderfield et al.*, 1999; *Walker et al.*, 2007], younger than the ^{14}C age of basement pore fluids to the west, although corrections for dispersion and mixing with much older water adjacent to the primary flow channels could significantly reduce age estimates (corrections by a factor of 10 to 1000 may be required for fluids flowing through heterogeneous, fractured rock systems) [*Sanford*, 1997; *Fisher et al.*, 2003b; *Stein and Fisher*, 2003].

Thermal and geochemical studies of Baby Bare outcrop and the plume of discharging fluid in the water column above the outcrop suggest a discharge rate of 5–20 kg/s [*Thomson et al.*, 1995; *Mottl et al.*, 1998; *Wheat et al.*, 2004]. The fluid discharge rate from Baby Bare may be somewhat higher than this, considering (a) the difficulties in estimating heat and fluid fluxes from a low-temperature plume, and (b) that extrapolating diffuse flow over the outcrop would tend to bias estimates toward lower rates if sites of focused flow were missed. While Baby Bare appears to act strictly as a site of discharge, subseafloor thermal measurements and pore fluid samples from Grizzly Bare show evidence for intraoutcrop discharge (outflow from an outcrop that originated as inflow to the same outcrop), in addition to recharge associated with interoutcrop flow [*Hutnak et al.*, 2006; *Wheat et al.*, 2013]. The vast majority of fluid discharging from Baby Bare flowed into the crust through Grizzly Bare [*Wheat et al.*, 2000; *Fisher et al.*, 2003b; *Hutnak et al.*, 2006]. Only a tiny fraction of Baby Bare discharge could have originated as slow infiltration through overlying sediments, and this process has never been detected in the field, despite geochemical sampling and thermal measurement at hundreds of locations. The minimum flow rate that is geochemically detectable from analysis of pore fluids from sediment cores is ~0.1 mm/yr [*Fisher*, 2004], but even flow rates this low cannot be sustained across this area given typical sediment thickness and properties, and differential pressures (several tens of kilopascal) measured with long-term borehole observatories in the region [*Davis and Becker*, 2004; *Spinelli et al.*, 2004; *Hutnak et al.*, 2006].

2. Methods

2.1. Model and Configuration

This study uses Finite Element Heat and Mass (FEHM), a node-centered porous flow simulator developed at Los Alamos National Laboratory [*Zyvoloski et al.*, 2011]. FEHM uses a finite-volume approach to represent

Table 1. Formation Properties Used in Coupled-Flow Simulations

	Porosity, n (Unitless)	Thermal Conductivity, λ (W/m K)	Permeability, k (m^2)
Sediment[a]	0.39 to 0.52	1.36 to 1.51	1.1×10^{-17} to 2.2×10^{-17}
Outcrop[b]	0.1	1.82	10^{-12} to 10^{-11}
Aquifer[b]	0.1	1.82	10^{-14} to 10^{-9}
Deep crust[b]	0.05	1.93	10^{-18}

[a]Values vary with depth and are consistent through all simulations. The relatively narrow range of sediment permeability applies to the full sediment column, representing a range at a smaller scale of several orders of magnitude.
[b]Values assigned homogeneously throughout each region.

properties and solve for coupled and transient fluid flow and heat transport. FEHM solutions are calculated using a fully implicit solver with upstream weighting. Model domains comprise a Delaunay mesh of tetrahedral elements constructed with LaGriT (Los Alamos Grid Toolbox) [*George*, 1997].

Physical formation properties (homogeneous and isotropic) are assigned as a single value within each section of basaltic crust (the crustal aquifer, low-permeability deeper crust, and each outcrop region) and varied within different sets of simulations. Properties for the sediment layer (porosity, thermal conductivity, and permeability) vary with depth to account for compaction and are constant with time. Representative depth-dependent functions are created for each property, then discretized, and assigned to nodes such that the cumulative effects of the sediment layer are consistent with field data (Figure S1 in the supporting information). A summary of physical formation property assignments for all simulations is presented in Table 1. Single-phase fluid properties (viscosity, density, and enthalpy) are calculated at each time step using a lookup table and bilinear interpolation [*Zyvoloski et al.*, 2011].

Simulation run times range from 10^5 to 10^6 years. This is sufficient in each case to achieve a dynamic steady state, wherein transient behaviors persist (e.g., mixed convection, unstable secondary convection, and local circulation) while recharge and discharge rates through outcrops stabilize to ±0.1% per kyr of simulation time. Internal mass balance errors reported by FEHM and calculated during solution iteration are ≪1%. All simulations presented begin with the initial temperature and pressure conditions for an active outcrop-to-outcrop hydrothermal siphon, consistent with field observations. Though a number of alternate initial conditions are possible, our focus is on the sustainability of dynamic conditions (rather than their evolution), and earlier results for similar conditions have been shown to be relatively insensitive to initial conditions [*Winslow and Fisher*, 2015].

2.2. Model Domain

Model grids are designed to represent the geometry, scale, and properties relevant to the outcrop-to-outcrop hydrothermal siphon system at the field site (Figure 2). This includes Grizzly Bare and Baby Bare outcrops, spaced 50 km apart, and an outer section of the crust that places domain boundaries 40 km from each outcrop center. The total model domain represents a 4 km thick section of the ocean crust (volcanic rock and overlying sediment), 130 km × 80 km in lateral extent, and is aligned with the long-edge parallel to the ridge axis. For convenience, we refer to the alignment of Grizzly Bare and Baby Bare in this study as "south-north" and the perpendicular direction as "east-west," although Baby Bare is actually oriented north 20°E from Grizzly Bare. The vertical structure of the crust is represented by a series of flat tabular layers, excepting the sediment and crustal sections associated with outcrop slopes. The sediment layer (450 m thick everywhere except above outcrop edifices) sits atop a permeable crustal aquifer (100–600 m, varies by simulation), with a relatively impermeable underlying crustal layer (3 km). This thick section at depth is important for allowing warping of conductive isotherms below the aquifer, which is part of the feedback in coupled fluid-heat transport in crustal systems.

The entire model domain comprises 397 k nodes and 2.2 M elements, representing ~4.2×10^4 km^3 of sediment and rock. Resolution is finest within the aquifer and outcrops (50 to 250 m node spacing) and is significantly coarser in the sediment (200 to 500 m spacing) and underlying massive basalt layer (150 m to 2 km spacing). Resolution is also somewhat lower in areas within 20 km of the edge of the model domain. A single grid is used for all simulations. Different aquifer thicknesses are represented by modifying properties in the crustal section, but node positions and spacing do not change. Tests were performed regarding the overall impact of resolution on simulation behavior (supporting information Figure S2), with the finding that the grid

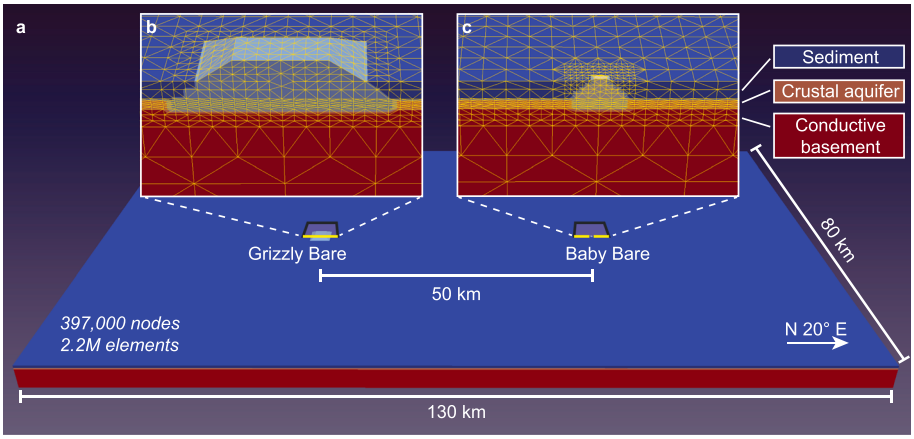

Figure 2. Model domain and grid geometry. (a) Full extent of model domain and dimensions. Layering shown is for 300 m thick aquifer, but thicker and thinner aquifers were tested as well. Thick yellow lines and boxes around outcrops depict cut planes and magnified regions (Figures 2b and 2c). (b) Magnified grid near Grizzly Bare, with cut plane through outcrop center. Yellow lines depict grid resolution, with nodes at intersections. Panel is 4 km across, with no vertical exaggeration. (c) Magnified grid near Baby Bare, with cut plane through outcrop center. Yellow lines depict grid resolution, with nodes at intersections. Same scale as Figure 2b.

resolution used in this study is high enough that flow on a regional scale (i.e., outcrop-to-outcrop, as part of the hydrothermal siphon) is generally unaffected by resolution. However, node spacing does influence the characteristics of flow behavior on smaller scales (e.g., mixed convection and intraoutcrop flow) and should be carefully considered when these scales are of primary interest.

The sides and bottom of the domain are closed to fluid flow, with time constant and depth-dependent hydrostatic pressure applied at the top (free flow) boundary. The side boundaries are also no flow, and a constant temperature boundary consistent with bottom water temperature (2°C) [*Davis et al.*, 1992; *Fisher et al.*, 2003b; *Hutnak et al.*, 2006] is applied to the top of the model domain. Basal heat input differs significantly from west to east due to the regional scale of the model domain and is specified as a function of crustal age, calculated based on a lithospheric cooling curve [*Stein and Stein*, 1992]. Basal heat flux values are lowered by ~15% relative to lithospheric to account for thermal rebound [*Hutnak and Fisher*, 2007], a process that is not explicitly modeled.

Simulations in the present study are similar in some ways to those shown in *Winslow and Fisher* [2015], but with important differences. The emphasis in the earlier study was on conditions that could sustain a hydrothermal siphon between two basement outcrops having three possible outcrop sizes. Formation properties were held constant, and outcrop properties were varied over a large range, with a focus on outcrop transmittance (permeability × outcrop surface area) in determining siphon sustainability and preferred flow direction. In contrast, the present study specifically emphasizes the field site near and around Grizzly Bare and Baby Bare, fixing outcrop sizes and exploring how varying other parameters influences the similarity of simulation results and field observations. Important observations used to check simulation applicability were described earlier, and metrics used to assess simulation suitability are described in the next section.

2.3. Metrics and Observational Constraints

For a simulation of the field site to be considered consistent with observational constraints, it must (1) sustain a hydrothermal siphon with recharge at Grizzly Bare in the south and discharge at Baby Bare in the north, (2) support siphon flow rates of 5–20 kg/s, and (3) have no measurable regional heat flux suppression at the seafloor beyond several kilometers from the edge of the recharging outcrop. Later in this study, we discuss the implications of relaxing these constraints, particularly the siphon flow rate. We create a series of parametric sets of simulations (Table 2), wherein a number of properties (e.g., upper crustal aquifer thickness and permeability of basaltic crust in either outcrop) are systematically tested. Simulation behavior for each set is assessed in terms of three model metrics, described below, and compared against observational constraints.

Siphon flow (Q_S) for each simulation is calculated by subtracting simulated recharge from discharge at Baby Bare, although simulated recharge through this feature is small (<1 kg/s in all simulations). This formulation is

Table 2. Geometry and Parameter Ranges Used in Parametric Tests

	Aquifer Thickness, b (m)	Aquifer Permeability, k_A (m^2)	Outcrop Permeability[a], k_G, k_B (m^2)	Modeled Dimensions	Crustal Flow to North of Baby Bare[b], Q_N (kg/s)
AQTEST	100	10^{-14} to 10^{-10}	10^{-12}	3-D	0
	200				
	300				
	600				
OCTEST	300	10^{-13} to 10^{-11}	10^{-12} to 10^{-11}	3-D	0
2DTEST[c]	300	10^{-13} to 10^{-9}	10^{-12}	2-D, 3-D	0
	600				
ADDQTEST	300	10^{-12} to 10^{-11}	10^{-12}	3-D	0 to 160

[a]Outcrop permeability is assigned homogeneously within the outcrop and underlying crustal rocks to the same depth as the crustal aquifer for each simulation.
[b]For crustal flow > 0, the specified flow leaves the model at the northern boundary of the aquifer. This process represents discharge through outcrops outside the model domain.
[c]Two-dimensional models are oriented in profile view, trending from Grizzly Bare to Baby Bare.

well justified because siphon recharge in the field occurs primarily through outcrops, with no chemically detectable recharge occurring though sediments. Thus, any discharge from Baby Bare that is in excess of outcrop-local recharge requires a commensurate rate of recharge at Grizzly Bare.

The siphon fraction (F_S), defined as the ratio of Q_S to the total simulated discharge from both outcrops, is used to quantify the relative significance of the hydrothermal siphon versus discharge supported by intraoutcrop circulation. When $F_S < 1$, intraoutcrop circulation occurs in one or both outcrops, in addition to recharge and discharge associated with the hydrothermal siphon.

The heat-suppression fraction (F_H) is used to quantify the extent to which regional seafloor heat flux is reduced below the background value that would be present in the absence of fluid flow, which is determined by completing a separate "conduction only" simulation with the same geometry and properties. We define F_H as the difference between this background value and the seafloor heat flux in the presence of fluid flow, normalized to the background value. This metric is used to assess the fraction of heat flux suppression over an entire simulation and can also be applied node-by-node across the top of the model domain to determine deviations in local heat flux. Seafloor heat flux values extending out to 2 km from the edge of each outcrop are excluded when assessing the regional seafloor heat flux deficit, as observations closer to outcrops are subject to the thermal influence of intraoutcrop circulation and conductive refraction [*Hutnak et al.*, 2006], and therefore are not representative of the background values. We consider simulations with F_H in excess of ±0.05 (a 5% deviation from the regional background) to be measurable in the field and thus inconsistent with observations. We sometimes present this metric as an absolute value, $|F_H|$, because deviations from background value can be either positive or negative.

3. Modeling Constraints on Crustal Properties and Flow Geometry

3.1. Flow Patterns in Coupled-Flow Simulations

In simulations with sustained hydrothermal siphons, fluid recharges at Grizzly Bare and flows northward through the upper crustal aquifer until discharging at Baby Bare, creating local (and measurable) thermal anomalies in the vicinity of each outcrop (Figure 3). The direction of flow between outcrops is controlled by the size and permeability of the outcrops [*Winslow and Fisher*, 2015] and is strongly favored from Grizzly Bare to Baby Bare at this field site. The general south-to-north flow pattern within the crustal aquifer comprises a dipole, with recharging fluid at Grizzly Bare that travels along both direct and indirect paths to Baby Bare (Figure 4a). While the most rapid flows follow relatively direct paths between the outcrops, a fraction of fluid travels on sweeping paths around and behind the outcrops. In addition, secondary (local) convection can cause small-scale flow in the crust in essentially any direction, including back toward a recharging outcrop or away from a discharging outcrop. Thus, the simulations show how an outcrop-to-outcrop hydrothermal siphon can coexist with local flow in the direction opposite to the primary siphon flow direction. The distribution and relative importance of specific flow paths will ultimately depend on the detailed nature of the permeability network present in the field, which is highly idealized in these simulations, but the possibility for fluids to take both direct and indirect paths appears to be a common characteristic of these systems, even without explicit heterogeneity in crustal properties.

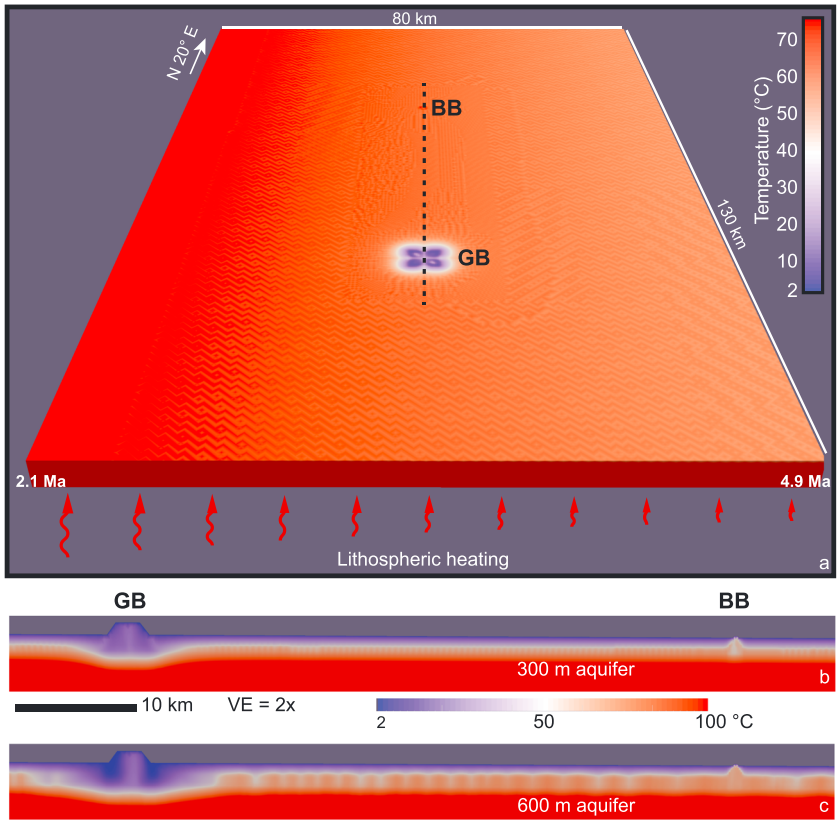

Figure 3. Simulation output showing temperatures at the top of the basement aquifer and along a profile through the aquifer. This simulation (part of the AQTEST set) has and $k_A = 3 \times 10^{-12}$ m^2. (a) Perspective view from the south, with $b = 300$ m. Colors show domain temperature at the top of the crustal aquifer (450 m below seafloor). Basal heat input is applied as a function of crustal age, resulting in west-to-east decrease in crustal temperatures across the model domain. Coolest and warmest temperatures are associated with hydrothermal recharge and discharge, respectively, through outcrops (GB = Grizzly Bare, BB = Baby Bare). Dotted line is 70 km long and shows location of model profiles shown in Figures 3b and 3c. (b) Cross-section profile through the upper 1.5 km of simulation having $b = 300$ m. Small-scale convection homogenizes basement temperatures as water flows from Grizzly Bare to Baby Bare. (c) Cross-section profile through the upper 1.5 km of simulation having $b = 600$ m. There is more rapid flow from Grizzly Bare to Baby Bare, but small-scale convection occurs within wider cells, leading to greater variability in seafloor heat flux, and a larger region of chilled basement rock around Grizzly Bare.

Local convection often occurs both in the aquifer between the outcrops and within the outcrops (Figures 3 and 4); most simulations include significant intraoutcrop flow at Grizzly Bare. In contrast, there is virtually no intraoutcrop circulation at Baby Bare; the vast majority of discharge through this outcrop comes from Grizzly Bare. Simulations typically include a temperature difference of ~50–60°C between recharging fluids at Grizzly Bare and discharging fluids at Baby Bare (Figures 3a and 3b), with differential pressure in the crustal aquifer between the two outcrops of 20–100 kPa (varies with depth and flow rate). These conditions generate lateral specific discharge (volume flow rate per cross-sectional area, m^3/m^2/yr = m/yr) within in the crustal aquifer of 0.2 to 3 m/yr directly between the two outcrops, indicating an outcrop-to-outcrop travel time of 2 to 25 kyr assuming plug flow and 10% effective porosity, or 0.2 to 2.5 kyr assuming 1% effective porosity. Specific discharge from the outcrops is more rapid (4 to 34 m/yr), with the highest flow rates in each simulation associated with outflow at Baby Bare. Flow through the sediments in all simulations is slow enough ($<$0.1 mm/yr) so as to be undetectable by thermal or geochemical methods, consistent with field observations.

Simulations include secondary rolls oriented parallel to the trend between Grizzly Bare and Baby Bare (Figures 3b and 3c). These rolls coalesce and break up during net transport from Grizzly Bare to Baby Bare, a form of mixed convection, and are smaller in cross section within simulations having a thinner aquifer. A thicker aquifer also results in a wider region of cooling below and adjacent to Grizzly Bare, extending $>$5 km from the outcrop edge. Additional secondary rolls occur with an orientation perpendicular to the

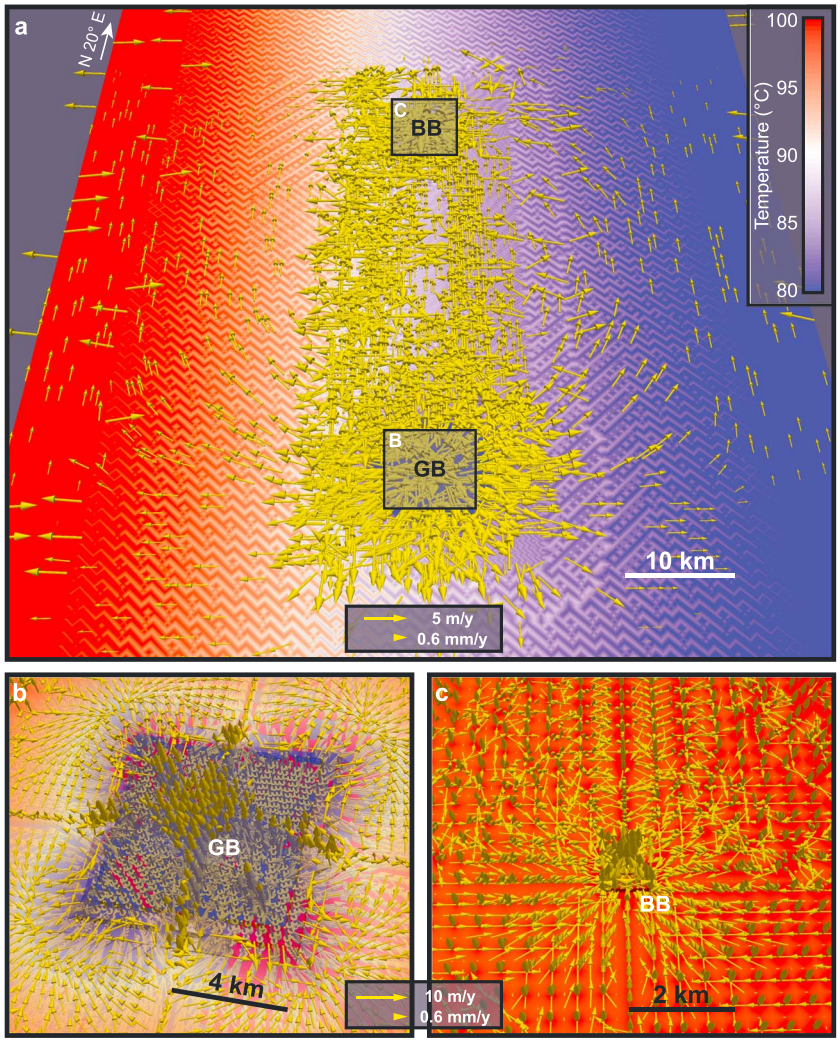

Figure 4. Three-dimensional patterns of hydrothermal circulation. Simulation with $b = 300$ m and $k_A = 3 \times 10^{-12}$ m^2, with sediment and uppermost basement layer removed, to make it easier to see flow vectors. (a) Colors show domain temperature at base of crustal aquifer, viewed from the south. The overall fluid flow pattern within the crustal aquifer is shown with only lateral (*X*-*Y*) fluid flow components, with vector lengths on a natural-log scale. Only 3% of the flow vectors are shown, selected randomly, for clarity. Vector density is higher near the center of the model domain where the grid resolution is finest. Shaded boxes depict magnified regions in Figures 4b and 4c. (b) Top-down perspective view (from the south) of three-dimensional flow pattern around and within Grizzly Bare outcrop, including recharge near outcrop corners and discharge near center. Flow vectors are plotted on a natural-log scale. (c) Top-down perspective view (from the south) of three-dimensional flow pattern in Baby Bare outcrop and surrounding aquifer, which is dominantly discharging. Flow vectors are plotted on a natural-log scale, as in Figure 4b.

north-south trend, including areas near the east and west boundaries of the domain (Figure 4a). Although rolls with this geometry may occur within the natural system, they are also influenced in our simulations by the presence of no-flow side boundaries. The focus of this study is on flow around and between the basement outcrops; larger and more detailed model domains, and additional observational constraints, will be needed to quantify and evaluate the nature of smaller-scale flow patterns in locations distant from the outcrops.

3.2. Siphon Dependence on Aquifer and Outcrop Properties

One set of simulations (AQTEST, Table 2) is designed to resolve the influence of permeability and the thickness of the upper crustal aquifer (k_A and b, respectively). In order to understand the combined effects of both properties on the behavior of the hydrothermal siphon, we present four model grids, with simulations spanning a range of aquifer thicknesses (100 to 600 m) and aquifer permeability (10^{-14} to 10^{-10} m^2). Outcrop permeability is assigned

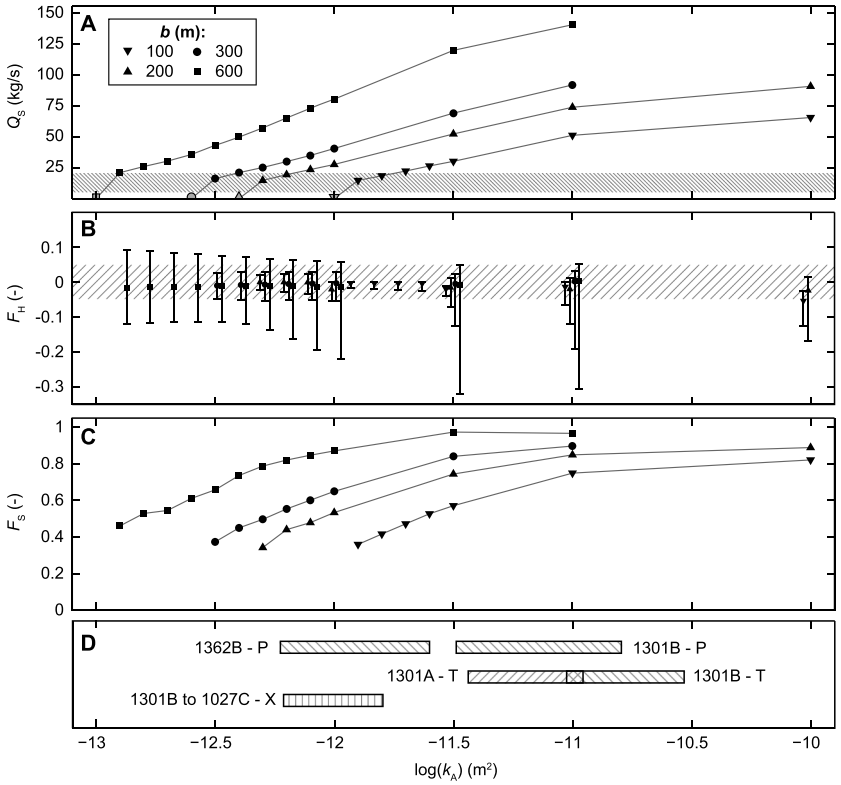

Figure 5. Results from AQTEST simulations and comparison with borehole data. (a) Siphon flow (Q_S) versus aquifer permeability, with symbol type differentiating aquifer thickness. Each symbol represents a single simulation, run to dynamic steady state. The shaded area is the range of discharge rates estimated for Baby Bare outcrop [*Thomson et al.*, 1995; *Mottl et al.*, 1998; *Wheat et al.*, 2004]. Grey symbols show the highest values of k_A for which the hydrothermal siphon fails. (b) Heat-suppression fraction (F_H) versus aquifer thickness and permeability. The shaded area highlights simulations with $|F_H| < 0.05$, satisfying observational constraints. Filled symbols indicate the mean values for seafloor nodes in each simulation, and the error bars indicate the 25th and 75th percentiles of seafloor values. Symbols are shifted slightly left or right for clarity. (c) Siphon fraction (F_S) versus aquifer thickness and permeability. In some simulations, there is as much (or more) fluid discharging locally through Grizzly Bare than there is continuing north to discharge through Baby Bare. (d) Summary of borehole permeability test results, where P = packer test, T = temperature log, and X = cross-hole response. Data are for test intervals of 100 to 600 m, taken from *Becker and Fisher* [2008] (Hole 1301B), *Fisher et al.* [2008] (Hole 1301B to 1027C), *Becker et al.* [2013] (Hole 1362B), and *Winslow et al.* [2013] (Holes 1301A and 1301B).

in a moderate value of 10^{-12} m^2 for all simulations; the impact of outcrop permeability is investigated later with OCTEST simulations (described in the next section). Hydrothermal siphon behavior for each simulation is summarized in terms of three metrics defined earlier (Figure 5): siphon discharge (Q_S), the fraction of regional heat flux suppression (F_H), and the fraction of outcrop discharge that is associated with the siphon (F_S).

All AQTEST simulations that sustain a hydrothermal siphon do so with Q_S at or above the observed rate of discharge from Baby Bare outcrop (5 to 20 kg/s) (Figure 5a). Most simulations produce flow rates of 25 to 150 kg/s, but results for a small number of simulations with $b \leq 300$ m have flow rates within the range constrained by observations (5 to 20 kg/s). All simulations with $b \leq 300$ m have minimal regional heat flux anomalies ($|F_H| < 0.05$), and local heat flux anomalies also fall within a narrow range (Figure 5b). Although mean F_H in simulations with $b = 600$ m falls within this threshold, local variability in all of these simulations far exceeds $F_H = 0.05$. This increased variability in heat flux results from a thicker aquifer generating larger temperature differences between the upward and downward limbs of local convection cells when $k_A = 10^{-13}$ to 10^{-12} m^2. With this range of properties, the convective pattern influences seafloor heat flux in ways inconsistent with field observations (background heat flux is relatively consistent).

The pattern of Q_S versus k_A is similar for each aquifer geometry, but the curves are shifted laterally (Figure 5a). Notably, the difference in k_A required to sustain a siphon is not proportional to the difference in b, as would be expected if transmissivity (aquifer hydraulic conductivity times layer thickness) were the only control: a

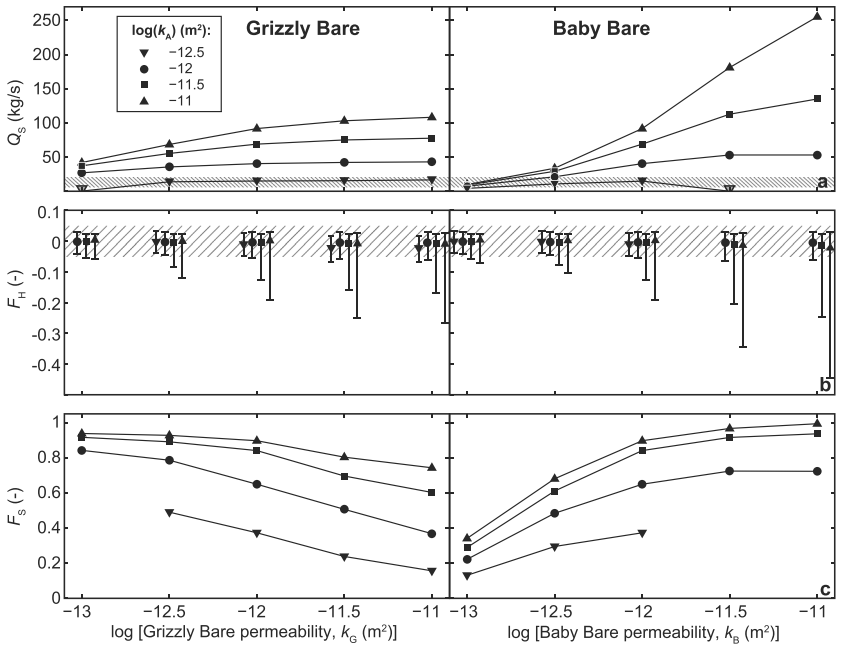

Figure 6. Results from OCTEST simulations for Grizzly Bare and Baby Bare. (a) Siphon flow (Q_S) versus outcrop permeability for each outcrop, with symbol type differentiating aquifer permeability. Each symbol represents a single simulation, run to dynamic steady state. The shaded area is the acceptable range of siphon flow established by observations [*Thomson et al.*, 1995; *Mottl et al.*, 1998; *Wheat et al.*, 2004]. (b) Heat-suppression fraction (F_H) versus outcrop and aquifer permeability. The shaded area highlights simulations with $|F_H| < 0.05$. Filled symbols indicate the mean values for seafloor nodes in each simulation, and the error bars indicate the 25th and 75th percentiles of seafloor values. Symbols are shifted slightly left or right for clarity. (c) Siphon fraction (F_S) versus outcrop and aquifer permeability.

100 m aquifer is one sixth as thick as a 600 m aquifer yet requires a tenfold increase in k_A to produce a similar rate of siphon flow. It appears that aquifer thickness influences the efficiency of heat extraction in two ways, affecting both transmissivity and the depth of circulation, with greater depth allowing a larger contrast in the temperature of recharging and discharging fluids, resulting in a greater pressure difference between the ends of the siphon [e.g., *Fisher et al.*, 2003b; *Fisher and Wheat*, 2010; *Anderson et al.*, 2013].

The next parametric set (OCTEST) focuses on the influence of permeability within Grizzly Bare (k_G) and Baby Bare (k_B) outcrops. We use a 300 m aquifer in all simulations and vary the properties of each outcrop separately (keeping k_G fixed at 10^{-12} m^2 while varying k_B, and vice versa). Four values of k_A are tested to assess the sensitivity of results to aquifer properties (Figure 6).

All OCTEST simulations have Q_S at or above rates estimated from field observations (5–20 kg/s), with a small number of simulations with low k_B ($1–3 \times 10^{-13}$ m^2) or low k_A (3×10^{-13} m^2) falling within this range. All simulations also have mean $|F_H| < 0.05$, although there is significant local heat flux suppression in the majority of simulations with $k_A > 10^{-12}$ m^2. Within the ranges tested, an increase in permeability results in monotonic increases in both siphon flow (Q_S) and local heat flux suppression (F_H), with siphon flow being more sensitive to k_B than to k_A or k_G. Higher k_B also leads to higher siphon fraction, while k_G has the opposite effect (Figure 6c). This difference is largely due to the size contrast between Grizzly Bare and Baby Bare: Grizzly Bare is better able to support secondary convection and simultaneous recharge and discharge because it is larger, whereas the smaller surface area of Baby Bare limits the formation of secondary convection, restricting the outcrop to discharge only. Changes in k_B only affect discharge, with Baby Bare acting solely as a discharge site in all OCTEST simulations, but increases in k_G amplify both recharge and discharge at Grizzly Bare and tend to increase intraoutcrop circulation more than they increase siphon flow (driving down F_S).

3.3. Discussion of Permeability and Aquifer Thickness

AQTEST simulation results show distinct behavior that varies with aquifer thickness, but the pattern and magnitude of both Q_S and F_S as a function of k_A are similar for each value of aquifer thickness (Figures 5a and 5c).

While variations in b shift these curves by up to an order of magnitude in k_A, the similarity of the Q_S versus b response makes it difficult to constrain the aquifer's thickness on the basis of these results alone. Borehole logs and results from packer testing show evidence for high permeability to a depth of ~320 m into the crust but also suggest that the upper extrusive ocean crust may comprise a series of thin, highly permeable units [*Becker et al.*, 2013; *Fisher et al.*, 2014]. While we did not explicitly model separate zones within a single aquifer, the fact that a number of simulations involving thin aquifers (100 m, 200 m) resulted in active hydrothermal siphons and were consistent with the field constraints suggests that thin zones are capable of supporting observed flows without violating field constraints. Results from the ensemble of AQTEST simulations suggest that the best match for aquifer thickness in this setting is $b < 600$ m. In addition, all simulations with $b = 600$ m had significant local seafloor heat flux anomalies (Figure 5b), including an area of suppressed seafloor heat flux that extends more than 5 km from the edge of Grizzly Bare. Neither of these heat flux characteristics is observed in the field [*Hutnak et al.*, 2006]. Secondary convection might be inhibited in simulations incorporating a thicker aquifer if small-scale layering (associated with individual flow units) were incorporated, either explicitly or by modeling a lower vertical permeability in the crustal aquifer. However, this approach would also restrict flow to and from outcrop edifices unless layering/anisotropy was omitted below these features.

AQTEST simulations that result in active hydrothermal siphons (including those with Q_S and/or F_H outside observational constraints) span 3 orders of magnitude in k_A (10^{-13} to 10^{-10} m^2). The span of permeability for simulations within observational constraints (Q_S from 5 to 20 kg/s, $|F_H| < 0.05$) is significantly narrower (<1 order of magnitude), with k_A ranging from 3×10^{-13} to 2×10^{-12} m^2. Both ranges overlap with estimates of permeability from borehole packer testing and thermal logs in the region [*Becker and Fisher*, 2008; *Becker et al.*, 2013; *Winslow et al.*, 2013] and bracket the value derived from a single cross-hole test [*Fisher et al.*, 2008] (Figure 5d). These calculations result in lower values of permeability than those inferred from earlier two-dimensional modeling of the same system [*Hutnak et al.*, 2006]; a more extensive comparison between two- and three-dimensional modeling results is presented later.

The hydraulic properties of basaltic rock outcrops on the seafloor are not well constrained by field data, and given complexities of drilling in bare rock settings, the rarity of field constraints on outcrop properties is likely to persist. However, modeling results, particularly those from OCTEST simulations, provide insight into permeability at the recharging and discharging end of this hydrothermal siphon (k_G and k_B). Simulations that have both high k_A and high outcrop permeability ($\geq 10^{-12}$ m^2) result in significantly greater Q_S and $|F_H|$ than observed at the field site. This shows that while permeability $\geq 10^{-12}$ m^2 is physically possible for a hydrothermal siphon such as that seen in this field area, elevated permeability both within the crust and within outcrops makes it more difficult to match field constraints.

Siphon flow in these simulations is more sensitive to changes in k_B than in k_G, suggesting that siphon behavior has greater dependence on properties near the site of discharge. The "discharge-dominated" nature of this system results from temperature being a primary control on driving forces that sustain the siphon. Recharging fluids enter at a fixed temperature (that of bottom water, ~2°C in this region), so the temperature of fluids in the discharging column ultimately sets the pressure difference (and thus the driving force) between the outcrops. That discharge temperatures, and thus driving forces, are inversely dependent on flow rates create a negative feedback that establishes a functional relationship between permeability and the rate of siphon flow. For example, a decrease in k_B slows fluid flow and increases the temperature of the fluid column at the discharge site, which in turn increases the differential pressure across the siphon and thereby increases flow rates. This process could diminish or even dominate the direct impact of reducing permeability. Discharge domination may be especially important because the natural hydrothermal siphon is close to failure in this case, with a small decrease in permeability causing the siphon to flow too slowly (or fail entirely, Figures 5 and 6). In addition, these simulations suggest that the permeability of basaltic outcrops in this setting may be less than or equal to that of the underlying aquifer. This could result from the nature of seamount construction, being less "layered" than the ocean crust in general, or perhaps because of sediment deposits that are emplaced prior to off-axis seamount formation.

On the basis of these initial results, additional parametric variations are explored based on "reference" simulations emphasizing aquifer thickness of $b = 300$–600 m, and aquifer and outcrop permeability of 10^{-13} to 10^{-11} m^2. This reduces the number of possible parameter combinations and allows direct comparison between reference simulation results and those associated with the options described in the next sections.

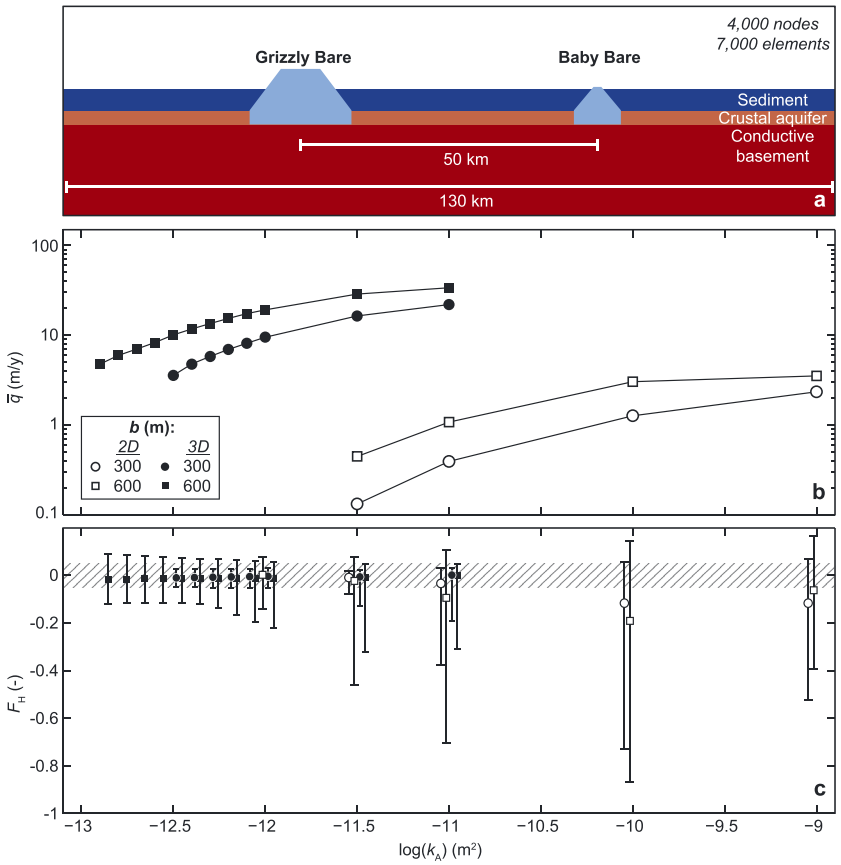

Figure 7. Results from 2DTEST simulations, contrasting dimensionality. (a) Geometry of 2-D simulations. Domain is that of a vertical cut plane through both outcrops along the 130 km length of the grid (Figure 2). (b) Mean specific discharge at Baby Bare ($\overline{q}$) versus aquifer permeability, with symbol type differentiating aquifer thickness. Open and closed symbols show results from two- and three-dimensional simulations, respectively. (c) Heat-suppression fraction (F_H) by aquifer thickness and permeability. The shaded area highlights simulations with $|F_H| < 0.05$. Symbols are shifted slightly left or right for clarity.

4. Comparison Between Two-Dimensional and Three-Dimensional Simulations

4.1. Siphon Response to Dimensionality

Here we present a parametric set of simulations performed in a two-dimensional (profile) geometry (2DTEST), which treats variations on both b and k_A in a similar fashion to AQTEST simulations. The two-dimensional geometry is that of a vertical cut plane along the 130 km length of the grid through the outcrop centers (Figure 7a). Volumetric flow, used elsewhere in this study to describe the magnitude of siphon flow, is not strictly defined for two-dimensional problems because volumes are inherently three-dimensional. Results in this section are instead presented in terms of mean specific discharge ($\overline{q}$), volume rate per cross-sectional area, evaluated at the surface of the Baby Bare outcrop. This metric has the benefit of being calculable for both two- and three-dimensional geometries, making it possible to compare results from similar simulations in each regime. In addition, we constrain realistic siphon behavior in two dimensions based on the system having an active hydrothermal siphon and negligible regional heat flux suppression, as applied for three-dimensional simulations.

Results for 2DTEST simulations are compared to a subset of AQTEST simulations with an equivalent three-dimensional geometry (Figure 7). A number of two-dimensional simulations sustain hydrothermal siphons and do so with the highest flow rates associated with discharge through Baby Bare, and similar values for temperature and differential pressures compared to those found in three-dimensional simulations. However, many flow behaviors found in three dimensions, including dipole flow and complex circulation within the Grizzly Bare outcrop (Figure 4b), are not possible in two dimensions. Simulations in two dimensions have significantly lower values of $\overline{q}$ (0.1 to 4 m/yr) than those for simulations in three dimensions with

commensurate properties (4 to 34 m/yr). Most two-dimensional simulations also produce extreme local variability in heat flux and lower mean values of F_H than do their three-dimensional counterparts, falling well outside the acceptable range of $|F_H| < 0.05$. 2DTEST simulations are also incapable of supporting hydrothermal siphons with lower values of k_A (10^{-13} to 10^{-12} m^2). That two-dimensional simulations require higher values of k_A to support hydrothermal siphons is consistent with higher property estimates found in the previous two-dimensional modeling of this system [*Hutnak et al.*, 2006].

4.2. Discussion of Dimensionality in Simulations

Representing outcrop-to-outcrop systems in two dimensions restricts possible flow patterns to those within the planar model domain, removing the possibility of dipole-like flow that is typical of simulations in three dimensions (Figure 4) and altering the character of local recharge and discharge within individual outcrops. This distinction results in large differences in both $\overline{q}$ and F_H due to the lack of flow paths outside of the primary flow plane. Forcing all siphon flow to travel through a planar feature results in hydrothermal cooling being focused into relatively small region, generating excessive heat flux suppression between the outcrops. This flow restriction also results in lower $\overline{q}$ because driving forces are similar in both two- and three-dimensional simulations, set by thermally derived pressure differences in the aquifer between the outcrops. These factors ultimately lead to higher simulated values of k_A (by 1 to 2 orders of magnitude) being required to sustain an outcrop-to-outcrop hydrothermal siphon in two dimensions.

The ratio of exposure areas of the two outcrops (A_B/A_G) is different for two- and three-dimensional simulations, even for an otherwise identical geometry. This ratio is approximately 1/100 for Baby Bare and Grizzly Bare in three dimensions but 1/10 in two dimensions. This ratio has been shown in earlier work to influence both siphon behavior and the property ranges capable of supporting an outcrop-to-outcrop hydrothermal siphon [*Winslow and Fisher*, 2015]. Though restricting the geometry to two dimensions affects a number of factors that may be important to overall siphon behavior (e.g., convection and dipole flow), the shift in A_B/A_G alone can explain why systems that support hydrothermal siphons in three dimensions are unable to do so in two dimensions.

Two- and three-dimensional simulations generate results that are quantitatively distinct. Explicitly representing the three-dimensional system geometry significantly influences the magnitude and behavior of siphon flow, produces separate trends in response to b and k_A, and alters the range of properties under which the hydrothermal siphon can operate. Given that simulations in three dimensions strictly improve on physical and geometric accuracy, these differences in behavior make a strong case for the necessity of three-dimensional modeling for evaluating ridge flank hydrothermal systems.

5. Influence of Additional Crustal Discharge North of Baby Bare

5.1. Siphon Response to Additional Crustal Discharge

Although this study focuses on the dipole system operating between the Grizzly Bare and Baby Bare outcrops, there are other outcrops in the region to the north and northeast: Mama Bare, Papa Bare, and Zona Bare [*Davis et al.*, 1992; *Wheat et al.*, 2000; *Hutnak et al.*, 2006]. Though there is no direct hydrologic evidence for a connection between the Grizzly Bare to Baby Bare system and other outcrops to the north, geochemical studies suggest that there is a systematic variation in basement fluid chemistry from Baby Bare to north of Mama Bare [*Wheat et al.*, 2000]. There is no estimate of the rate of fluid discharge at the outcrops north of Baby Bare outcrop, but it remains possible that some fluid recharging through Grizzly Bare bypasses Baby Bare and discharges through one or more of the northern features. We explore the potential impact of this additional flow with the ADDQTEST simulations (Table 2). In these simulations, we assess the quantity of hydrothermal fluid that could recharge at Grizzly Bare and then flow past and north of Baby Bare, without perturbing the discharge at Baby Bare beyond what is allowed by observational constraints.

To represent the influence of additional discharge north of Baby Bare (Q_N), we include a fluid sink within the upper aquifer at the northern boundary of the domain. We use this sink to remove water from the domain at a series of specified rates and assess the quantitative impact on flow between Grizzly Bare and Baby Bare. As in the earlier simulations, the model domain extends 40 km to the south and north of Grizzly Bare to Baby Bare outcrops, respectively, placing the domain boundaries far from the primary flow paths of interest. A fully coupled representation of additional outcrops is difficult to justify given the lack of information on flow rates

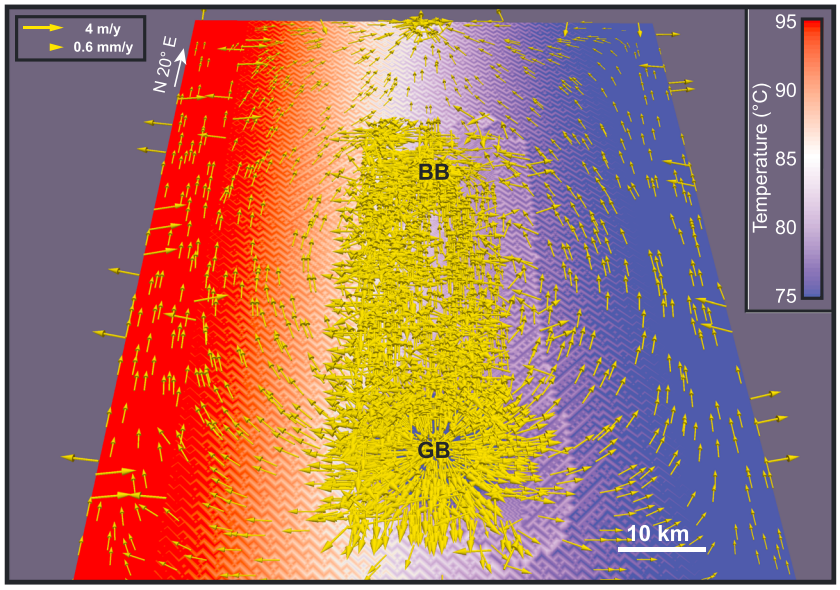

Figure 8. Flow pattern with additional discharge north of Baby Bare, viewed from the south. This simulation has additional outflow at the northern edge of the domain (part of ADDQTEST), with $Q_N = 40$ kg/s, $b = 300$ m, and $k_A = 10^{-12}$ m^2. Colors show domain temperature (75 to 95°C) at the base of the aquifer (note 5°C offset in color scaling compared to Figure 4, because there is a greater net flow through the crustal aquifer, and thus more advective heat extraction). Flow vectors include only lateral (*X*-*Y*) components, with lengths on a natural-log scale. Only 3% of the flow vectors are shown, selected randomly, for clarity. Vector density is higher near the center of the model domain where the grid resolution is finest.

and patterns north of Baby Bare and would require a commensurately larger model domain (including expansion in east-west width to accommodate greater north-south dimensions while preserving the flow dipole). This would also result in modeling of a fundamentally different system than that used in earlier simulations, making direct comparison difficult. We avoid these complexities by retaining a model domain identical to that used earlier studies and imposing a fluid sink as a simple parameterization.

Typical flow patterns in ADDQTEST simulations (Figure 8) are similar to those seen in simulations without additional flow to the north (Figure 4), including a mixture of regional and local flow systems and characteristic rates of specific discharge (scaling with the mass flux). Temperatures in the crustal aquifer are about 5°C cooler in this example compared to the simulation without additional discharge to the north (Figure 4), because there is a greater net flow of water through the crust and commensurately greater efficiency in advection of lithospheric heat. Flow rates to the east and west of the outcrops are somewhat higher in ADDQTEST simulations, in response to greater overall throughput of crustal fluid that distributes the thermal influence of the hydrothermal siphon over a larger area. In addition, the northward fluid paths bifurcate near Baby Bare outcrop, separating fluids that become Baby Bare discharge from those flowing to the northern outcrop. The specific pattern varies with overall system flow rates, and with the parameterization used to represent additional outcrop discharge, but similar behaviors (greater flow rates along longer flow paths and bifurcation in flow paths) are present in all simulations with additional discharge to the north.

To illustrate the influence of additional fluid discharge to the north of Baby Bare outcrop, we consider three sets of ADDQTEST simulations having different aquifer permeability values (Table 2 and Figure 9). Each case uses a 300 m aquifer and a moderate permeability assignment for both outcrops ($k_G = k_B = 10^{-12}$ m^2). Hydrothermal siphons appear to be supportable for any value of Q_N provided that Q_S stays above ~15 kg/s, consistent with field observations. Below this threshold, the siphon fails and Baby Bare becomes a site of recharge for fluids flowing to the north, violating observational constraints. Most simulations resulting in hydrothermal siphons between Grizzly Bare and Baby Bare have Q_S above observed siphon discharge from Baby Bare, with two simulations near the upper end of this range (17 and 21 kg/s). All ADDQTEST simulations have mean $|F_H| < 0.05$, but though those with $k_A > 10^{-12}$ m^2 have significant local deviations in seafloor heat flux for all values of Q_N tested. Increases in Q_N result in monotonic decreases in Q_S, but result in

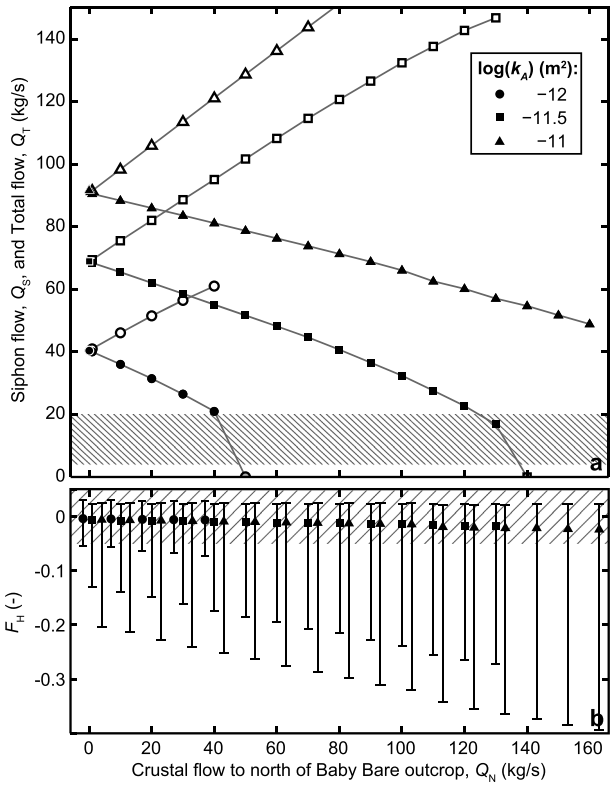

Figure 9. Results from ADDQTEST simulations: additional northern discharge. (a) Flow rate versus the rate of discharge north of Baby Bare (Q_N), with symbol type differentiating aquifer permeability. Closed symbols show Q_S only, and open symbols show the total flow through the system ($Q_T = Q_S + Q_N$). Grey symbols show the minimum Q_N for which the hydrothermal siphon fails. The shaded area indicates range of discharge rates estimated for Baby Bare [*Thomson et al.*, 1995; *Mottl et al.*, 1998; *Wheat et al.*, 2004]. (b) Heat-suppression fraction (F_H) versus and aquifer permeability. The shaded area highlights simulations with $|F_H| < 0.05$. Symbols are shifted slightly left or right for clarity.

greater total flow through the system ($Q_T = Q_N + Q_S$). Both responses (Q_S versus Q_N; Q_T versus Q_N) follow linear trends with slopes dependent on k_A (Figure 9a).

5.2. Discussion of Simulations With Additional Crustal Discharge

As an ensemble, ADDQTEST simulations demonstrate that a significant quantity of additional northern discharge (>40 kg/s) can occur contemporaneously with siphon flow between Grizzly Bare and Baby Bare, but only a narrow range of conditions is consistent with observational constraints. A number of simulations with $k_A = 10^{-12}$ m^2 fall close to the limit of constrained behavior, having both low heat flux suppression and Q_S above (but near) the observed range. In some of these cases, Q_N is larger than Q_S, suggesting that it is possible that more water recharged at Grizzly Bare is discharged north of Baby Bare than through Baby Bare itself. For simulations with $k_A = 10^{-12}$ m^2, the slope (dQ_S/dQ_N) is ~ −0.5, meaning that half of the fluid flowing to Q_N is drawn from the siphon, reducing siphon discharge from Baby Bare, Q_S, whereas the other half comes from an increase in recharge at Grizzly Bare. This result illustrates how multiple discharging (and perhaps recharging) outcrops may respond as a network to perturbations in flow conditions within one part of the hydrologic system.

Larger flows are possible in the ADDQTEST simulations compared to the AQTEST simulations without a significant increase in mean values of F_H, because flow in the crust north of Baby Bare is distributed across a broad area (Figure 8a). This generates a relatively modest seafloor heat flux anomaly. The impact of additional fluid flow on local heat flux suppression might be even smaller if Q_N were divided among multiple discharge sites (e.g., outcrops and exposed faults) or could be enhanced if flow in the crust were concentrated along a small number of discrete fractures or horizons [*Fisher et al.*, 1994; *Fisher and Becker*, 2000; *Spinelli and Fisher*, 2004]. In summary, ADDQTEST simulations suggest that significant flow from Grizzly Bare can continue to the north of Baby Bare, without causing the Grizzly Bare-to-Baby Bare hydrothermal siphon to fail. However, additional observations will be needed from the region north of Baby Bare to quantify flow rates and patterns with greater confidence, including a careful assessment of geochemistry to assess continuity in fluid evolution along this path, and independent determinations of rates of fluid discharge from additional outcrops.

6. Summary and Conclusions

The simulations presented in this study help to constrain the hydrologic properties and flow conditions (rates and patterns) within young crust on the eastern flank of the Juan de Fuca Ridge. In general, simulations with $k_A > 10^{-13}$ m^2 can sustain outcrop-to-outcrop hydrothermal siphons, and systems having k_A from 3×10^{-13} to 2×10^{-12} m^2 are most consistent with observational constraints (fluid flow rates and seafloor heat flux). A similar

range of properties also applies to the outcrops at both ends of the hydrothermal siphon, and simulations with higher values for k_A and either k_G or k_B (10^{-12} to 10^{-11} m^2) tend to result in heat flux suppression and siphon flow considerably greater than observed. If discharge from Baby Bare was somewhat higher than previously estimated, the range for aquifer permeability would be commensurately wider (for example, 3×10^{-13} to 10^{-11} m^2 for $Q_S \leq 75$ kg/s). Simulations with 600 m thick aquifers form hydrothermal siphons with somewhat lower values of k_A but typically have more variability in the seafloor heat flux anomaly than has been observed in the field (because a thicker aquifer permits more vigorous local mixing) and include much more heat flux suppression around Grizzly Bare outcrop than is observed. Thus, simulations having thinner aquifers ($b \leq 300$ m) provide a better overall match to field observations.

We found significant differences between two-dimensional and three-dimensional simulations in their ability to match field constraints, including flow rates and patterns, and the extent of seafloor heat flux variability. Because these quantitative observations constitute important constraints on system behavior, three-dimensional simulations are better suited for comparison with the natural system. A two-dimensional geometry is also incapable of representing azimuthal anisotropy and less suitable for incorporating realistic heterogeneity, bathymetry, or property boundaries. The geometry and processes intrinsic to outcrop-to-outcrop hydrothermal siphons, even those involving only two outcrops, are unequivocally three-dimensional in nature, based on both model results (e.g., Figure 4) and field observations [*Wheat et al.*, 2000, 2013; *Fisher et al.*, 2003b; *Hutnak et al.*, 2006].

Our simulations show that flow paths associated with a hydrothermal siphon are frequently indirect, combining outcrop-to-outcrop flow (in the form of a dipole) with smaller-scale convection that is oriented both along the trend between the outcrops and perpendicular to this path (Figures 4 and 8). These complex flow geometries will result in mixing of waters having different water-rock-heat histories (conditions and reaction times), even in simulations based on a relatively homogeneous crustal aquifer, as in the present paper. Adding permeability heterogeneity and anisotropy is likely to result in even greater variability in fluid residence times and physical conditions. There are additional challenges in representing long-term, transient system responses to changes in hydrothermal conditions, including sedimentation that leads to outcrop burial, and geologically justified initial conditions.

The simulations in the present study were designed to assess properties and processes in a specific region, where the background heat flux is very close to that predicted by lithospheric cooling curves and thus where basement thermal conditions are anomalously warm for a young ridge flank. This is an important site to model because there are so many observational constraints that help to identify which simulations are consistent with field conditions. In addition, many physical characteristics of this system are found in other locations: hundreds of meters of basement relief, thick sediments above a volcanic crustal aquifer, and tens of kilometers between pairs of basement outcrops. Given that heat flux constraints for this site are most often violated in simulations with thicker (>300 m) and more permeable ($>10^{-12}$ m^2) aquifers, it is likely that outcrop-to-outcrop hydrothermal siphons that extract significant lithospheric heat have one or both of these characteristics. Alternatively, it may be possible to simply increase the amount of fluid circulating through the crust with additional outcrops and/or shorter spacing between outcrops, both of which appear to have occurred at this site in the past [*Hutnak and Fisher*, 2007] and to be common characteristics of ridge flanks on a global basis [*Anderson et al.*, 2012].

Future modeling should improve the representation of geological variability within three-dimensional domains. Simulations should include a more realistic treatment of bathymetry and basement relief, which is known to influence flow and transport patterns [*Hartline and Lister*, 1981; *Fisher et al.*, 1990; *Wang et al.*, 1997; *Bani-Hassan et al.*, 2012]. Simulations with more complex distributions of crustal properties (heterogeneity and anisotropy) will introduce additional free parameters and increase computational demands. Models should eventually incorporate reactive transport, at which time the composition of fluids sampled from Baby Bare may be used as an observational constraint to test simulation applicability. More complex models will also require visualization of intricate and highly transient flow patterns but are likely to provide useful insights that can guide future field studies.

Acknowledgments
This research used data provided by the Ocean Drilling Program (ODP) and the Integrated Ocean Drilling Program (IODP) and was supported by National Science Foundation grants OIA-0939564, OCE-1031808, and OCE-1260408, and Consortium for Ocean Leadership Projects T327A7 and T327B7 (A.T.F.). We thank L. Coogan and two anonymous reviewers for their helpful suggestions that improved this paper. This is C-DEBI contribution 316.

References

Alt, J. C. (2004), Alteration of the upper oceanic crust: Mineralogy, chemistry, and processes, in *Hydrogeology of the Oceanic Lithosphere*, edited by E. E. Davis and H. Elderfield, pp. 456–488, Cambridge Univ. Press, Cambridge, U. K.

Anderson, B. W., L. A. Coogan, and K. M. Gillis (2012), The role of outcrop-to-outcrop fluid flow in off-axis oceanic hydrothermal systems under abyssal sedimentation conditions, *J. Geophys. Res.*, *117*, B05103, doi:10.1029/2011JB009052.

Anderson, B. W., K. M. Gillis, and L. A. Coogan (2013), A hydrologic model for the uppermost oceanic crust constrained by temperature estimates from carbonate minerals, *J. Geophys. Res. Solid Earth*, *118*, 3917–3930, doi:10.1002/jgrb.50325.

Anderson, R., M. Zoback, S. Hickman, and R. Newmark (1985), Permeability versus depth in the upper oceanic crust: In-situ measurements in DSDP Hole 504B, eastern equatorial Pacific, *J. Geophys. Res.*, *90*(NB5), 3659–3669, doi:10.1029/JB090iB05p03659.

Bani-Hassan, N., K. Iyer, L. H. Rüpke, and A. Borgia (2012), Controls of bathymetric relief on hydrothermal fluid flow at mid-ocean ridges, *Geochem. Geophys. Geosyst.*, *13*, Q05002, doi:10.1029/2012GC004041.

Bartetzko, A. (2005), Effect of hydrothermal ridge flank alteration on the in situ physical properties of uppermost oceanic crust, *J. Geophys. Res.*, *110*, B06203, doi:10.1029/2004JB003228.

Becker, K. (1989), Measurements of the permeability of the sheeted dikes in Hole 504B, ODP Leg 111, edited by E. K. Mazzullo et al., *Proc. Ocean Drill. Program Sci. Results*, *111*, 317–325.

Becker, K. (1996), Permeability measurements in Hole 896A and implications for the lateral variability of upper crustal permeability at sites 504 and 896, edited by J. C. Alt et al., *Proc. Ocean Drill. Program Sci. Results*, *148*, 353–363.

Becker, K., and A. T. Fisher (2008), Borehole packer tests at multiple depths resolve distinct hydrologic intervals in 3.5-Ma upper oceanic crust on the eastern flank of Juan de Fuca Ridge, *J. Geophys. Res.*, *113*, B07105, doi:10.1029/2007JB005446.

Becker, K., and E. E. Davis (2003), New evidence for age variation and scale effects of permeabilities of young oceanic crust from borehole thermal and pressure measurements, *Earth Planet. Sci. Lett.*, *210*(3-4), 499–508, doi:10.1016/S0012-821X(03)00160-2.

Becker, K., A. T. Fisher, and T. Tsuji (2013), New packer experiments and borehole logs in upper oceanic crust: Evidence for ridge-parallel consistency in crustal hydrogeological properties, *Geochem. Geophys. Geosyst.*, *14*, 2900–2915, doi:10.1002/ggge.20201.

Becker, N. C., C. G. Wheat, M. J. Mottl, J. L. Karsten, and E. E. Davis (2000), A geological and geophysical investigation of Baby Bare, locus of a ridge flank hydrothermal system in the Cascadia Basin, *J. Geophys. Res.*, *105*(B10), 23,557–23,568, doi:10.1029/2000JB900204.

Cowen, J. P., S. J. Giovannoni, F. Kenig, H. P. Johnson, D. Butterfield, M. S. Rappe, M. Hutnak, and P. Lam (2003), Fluids from aging ocean crust that support microbial life, *Science*, *299*(5603), 120–123, doi:10.1126/science.1075653.

Davis, E. E., and K. Becker (2004), Observations of temperature and pressure: Constraints on ocean crustal hydrologic state, properties, and flow, in *Hydrogeology of the Oceanic Lithosphere*, edited by E. E. Davis and H. Elderfield, pp. 225–271, Cambridge Univ. Press, Cambridge, U. K.

Davis, E. E., D. S. Chapman, K. Wang, H. Villinger, A. T. Fisher, S. W. Robinson, J. Grigel, D. Pribnow, J. Stein, and K. Becker (1999), Regional heat flow variations across the sedimented Juan de Fuca Ridge eastern flank: Constraints on lithospheric cooling and lateral hydrothermal heat transport, *J. Geophys. Res.*, *104*(B8), 17,675–17,688, doi:10.1029/1999JB900124.

Davis, E., et al. (1992), Flankflux: An experiment to study the nature of hydrothermal circulation in young oceanic-crust, *Can. J. Earth Sci.*, *29*(5), 925–952, doi:10.1139/e92-078.

De Villiers, S., and B. K. Nelson (1999), Detection of low-temperature hydrothermal fluxes by seawater Mg and Ca anomalies, *Science*, *285*(5428), 721–723, doi:10.1126/science.285.5428.721.

Edwards, K. J., W. Bach, and T. M. McCollom (2005), Geomicrobiology in oceanography: Microbe-mineral interactions at and below the seafloor, *Trends Microbiol.*, *13*(9), 449–456, doi:10.1016/j.tim.2005.07.005.

Elderfield, H., C. G. Wheat, M. J. Mottl, C. Monnin, and B. Spiro (1999), Fluid and geochemical transport through oceanic crust: A transect across the eastern flank of the Juan de Fuca Ridge, *Earth Planet. Sci. Lett.*, *172*(1), 151–165.

Fisher, A. T. (2004), Rates and patterns of fluid circulation, in *Hydrogeology of the Oceanic Lithosphere*, edited by E. E. Davis and H. Elderfield, pp. 339–377, Cambridge Univ. Press, Cambridge, U. K.

Fisher, A. T., and C. G. Wheat (2010), Seamounts as conduits for massive fluid, heat, and solute fluxes on ridge flanks, *Oceanography*, *23*(1), 74–87.

Fisher, A. T., and K. Becker (2000), Channelized fluid flow in oceanic crust reconciles heat-flow and permeability data, *Nature*, *403*(6765), 71–74, doi:10.1038/47463.

Fisher, A. T., K. Becker, and E. E. Davis (1997), The permeability of young oceanic crust east of Juan de Fuca Ridge determined using borehole thermal measurements, *Geophys. Res. Lett.*, *24*(11), 1311–1314, doi:10.1029/97GL01286.

Fisher, A. T., C. A. Stein, R. N. Harris, K. Wang, E. A. Silver, M. Pfender, M. Hutnak, A. Cherkaoui, R. Bodzin, and H. Villinger (2003a), Abrupt thermal transition reveals hydrothermal boundary and role of seamounts within the Cocos Plate, *Geophys. Res. Lett.*, *30*(11, 1550), doi:10.1029/2002GL016766.

Fisher, A. T., et al. (2003b), Hydrothermal recharge and discharge across 50 km guided by seamounts on a young ridge flank, *Nature*, *421*(6923), 618–621, doi:10.1038/nature01352.

Fisher, A. T., E. E. Davis, and K. Becker (2008), Borehole-to-borehole hydrologic response across 2.4 km in the upper oceanic crust: Implications for crustal-scale properties, *J. Geophys. Res.*, *113*, B07106, doi:10.1029/2007JB005447.

Fisher, A. T., J. C. Alt, and W. Bach (2014), Hydrogeologic properties, processes and alteration in the igneous ocean crust, in *Earth and Life Processes Discovered From the Subseafloor Environment—A Decade of Science Achieved by the Integrated Ocean Drilling Program (IODP)*, edited by R. Stein et al., pp. 507–551, Elsevier, New York.

Fisher, A., K. Becker, T. Narasimhann, M. Langseth, and M. Mottl (1990), Passive, off-axis convection through the southern flank of the Costa-Rica rift, *J. Geophys. Res.*, *95*(B6), 9343–9370, doi:10.1029/JB095iB06p09343.

Fisher, A., K. Becker, and T. Narasimhann (1994), Off-axis hydrothermal circulation: Parametric tests of a refined model of processes at deep-sea Drilling Project/Ocean Drilling Program Site 504, *J. Geophys. Res.*, *99*(B2), 3097–3121, doi:10.1029/93JB02741.

George, D. C. (1997), Unstructured 3D grid toolbox for modeling and simulation, LA-UR-97-3052, Los Alamos Grid Toolbox (LaGriT). [Available at http://lagrit.lanl.gov.]

Hartline, B., and C. Lister (1981), Topographic forcing of supercritical convection in a porous-medium such as the ocean crust, *Earth Planet. Sci. Lett.*, *55*(1), 75–86, doi:10.1016/0012-821X(81)90088-1.

Hasterok, D. (2013a), A heat flow based cooling model for tectonic plates, *Earth Planet. Sci. Lett.*, *361*, 34–43, doi:10.1016/j.epsl.2012.10.036.

Hasterok, D. (2013b), Global patterns and vigor of ventilated hydrothermal circulation through young seafloor, *Earth Planet. Sci. Lett.*, *380*, 12–20, doi:10.1016/j.epsl.2013.08.016.

Hutnak, M., and A. T. Fisher (2007), Influence of sedimentation, local and regional hydrothermal circulation, and thermal rebound on measurements of seafloor heat flux, *J. Geophys. Res.*, *112*, B12101, doi:10.1029/2007JB005022.

Hutnak, M., A. T. Fisher, L. Zuhlsdorff, V. Spiess, P. H. Stauffer, and C. W. Gable (2006), Hydrothermal recharge and discharge guided by basement outcrops on 0.7–3.6 Ma seafloor east of the Juan de Fuca Ridge: Observations and numerical models, *Geochem. Geophys. Geosyst.*, *7*, Q07O02, doi:10.1029/2006GC001242.

Hutnak, M., A. T. Fisher, R. Harris, C. Stein, K. Wang, G. Spinelli, M. Schindler, H. Villinger, and E. Silver (2008), Large heat and fluid fluxes driven through mid-plate outcrops on ocean crust, *Nat. Geosci.*, *1*(9), 611–614, doi:10.1038/ngeo264.

Karsten, J. L., N. Becker, M. J. Mottl, and C. G. Wheat (1998), Petrology of Baby Bare and Mama Bare lavas, *Geophys. Res. Lett.*, *25*(1), 117–120, doi:10.1029/97GL53564.

Kim, S.-S., and P. Wessel (2011), New global seamount census from altimetry-derived gravity data: New global seamount census, *Geophys. J. Int.*, *186*(2), 615–631, doi:10.1111/j.1365-246X.2011.05076.x.

Mottl, M. J., et al. (1998), Warm springs discovered on 3.5 Ma oceanic crust, eastern flank of the Juan de Fuca Ridge, *Geology*, *26*(1), 51–54, doi:10.1130/0091-7613(1998)026<0051:WSDOMO>2.3.CO;2.

Parsons, B., and J. G. Sclater (1977), Analysis of variation of ocean-floor bathymetry and heat-flow with age, *J. Geophys. Res.*, *82*(5), 803–827, doi:10.1029/JB082i005p00803.

Sanford, W. E. (1997), Correcting for diffusion in carbon-14 dating of ground water, *Ground Water*, *35*(2), 357–361, doi:10.1111/j.1745-6584.1997.tb00093.x.

Spinelli, G. A., and A. T. Fisher (2004), Hydrothermal circulation within topographically rough basaltic basement on the Juan de Fuca Ridge flank, *Geochem. Geophys. Geosyst.*, *5*, Q02001, doi:10.1029/2003GC000616.

Spinelli, G. A., E. G. Giambalvo, and A. T. Fisher (2004), Sediment permeability, distribution, and influence on fluxes in oceanic basement, in *Hydrogeology of the Oceanic Lithosphere*, edited by E. E. Davis and H. Elderfield, pp. 151–188, Cambridge Univ. Press, Cambridge, U. K.

Stein, C., and S. Stein (1992), A model for the global variation in oceanic depth and heat-flow with lithospheric age, *Nature*, *359*(6391), 123–129, doi:10.1038/359123a0.

Stein, C., and S. Stein (1994), Constraints on hydrothermal heat-flux through the oceanic lithosphere from global heat-flow, *J. Geophys. Res.*, *99*(B2), 3081–3095, doi:10.1029/93JB02222.

Stein, J. S., and A. T. Fisher (2003), Observations and models of lateral hydrothermal circulation on a young ridge flank: Numerical evaluation of thermal and chemical constraints, *Geochem. Geophys. Geosyst.*, *4*(3), 1026, doi:10.1029/2002GC000415.

Thomson, R. E., E. E. Davis, and B. J. Burd (1995), Hydrothermal venting and geothermal heating in Cascadia Basin, *J. Geophys. Res.*, *100*(B4), 6121–6141, doi:10.1029/95JB00030.

Underwood, M. B., K. D. Hoke, A. T. Fisher, E. E. Davis, E. Giambalvo, L. Zuhlsdorff, and G. A. Spinelli (2005), Provenance, stratigraphic architecture, and hydrogeologic influence of turbidites on the mid-ocean ridge flank of northwestern Cascadia Basin, Pacific Ocean, *J. Sediment. Res.*, *75*(1), 149–164, doi:10.2110/jsr.2005.012.

Villinger, H., I. Grevemeyer, N. Kaul, J. Hauschild, and M. Pfender (2002), Hydrothermal heat flux through aged oceanic crust: Where does the heat escape? *Earth Planet. Sci. Lett.*, *202*(1), 159–170, doi:10.1016/S0012-821X(02)00759-8.

Walker, B. D., M. D. McCarthy, A. T. Fisher, and T. P. Guilderson (2007), Dissolved inorganic carbon isotopic composition of low-temperature axial and ridge-flank hydrothermal fluids of the Juan de Fuca Ridge, *Mar. Chem.*, *108*(1-2), 123–136, doi:10.1016/j.marchem.2007.11.002.

Wang, K. L., J. H. He, and E. E. Davis (1997), Influence of basement topography on hydrothermal circulation in sediment-buried igneous oceanic crust, *Earth Planet. Sci. Lett.*, *146*(1-2), 151–164, doi:10.1016/S0012-821X(96)00213-0.

Wheat, C. G., and M. J. Mottl (2000), Composition of pore and spring waters from Baby Bare: Global implications of geochemical fluxes from a ridge flank hydrothermal system, *Geochim. Cosmochim. Acta*, *64*(4), 629–642, doi:10.1016/S0016-7037(99)00347-6.

Wheat, C. G., and M. J. Mottl (2004), Geochemical fluxes through mid-ocean ridge flanks, in *Hydrogeology of the Oceanic Lithosphere*, edited by E. E. Davis and H. Elderfield, pp. 627–658, Cambridge Univ. Press, Cambridge, U. K.

Wheat, C. G., H. Elderfield, M. J. Mottl, and C. Monnins (2000), Chemical composition of basement fluids within an oceanic ridge flank: Implications for along-strike and across-strike hydrothermal circulation, *J. Geophys. Res.*, *105*(B6), 13,437–13,447, doi:10.1029/2000JB900070.

Wheat, C. G., H. W. Jannasch, M. Kastner, J. N. Plant, and E. H. DeCarlo (2003), Seawater transport and reaction in upper oceanic basaltic basement: Chemical data from continuous monitoring of sealed boreholes in a ridge flank environment, *Earth Planet. Sci. Lett.*, *216*(4), 549–564, doi:10.1016/S0012-821X(03)00549-1.

Wheat, C. G., M. J. Mottl, A. T. Fisher, D. Kadko, E. E. Davis, and E. Baker (2004), Heat flow through a basaltic outcrop on a sedimented young ridge flank, *Geochem. Geophys. Geosyst.*, *5*, Q12006, doi:10.1029/2004GC000700.

Wheat, C. G., H. W. Jannasch, A. T. Fisher, K. Becker, J. Sharkey, and S. Hulme (2010), Subseafloor seawater-basalt-microbe reactions: Continuous sampling of borehole fluids in a ridge flank environment: Subseafloor borehole fluids, *Geochem. Geophys. Geosyst.*, *11*, Q07011, doi:10.1029/2010GC003057.

Wheat, C. G., S. M. Hulme, A. T. Fisher, B. N. Orcutt, and K. Becker (2013), Seawater recharge into oceanic crust: IODP Exp 327 Site U1363 Grizzly Bare Outcrop: Seawater recharge into basaltic crust, *Geochem. Geophys. Geosyst.*, *14*, 1957–1972, doi:10.1002/ggge.20131.

Winslow, D. M., and A. T. Fisher (2015), Sustainability and dynamics of outcrop-to-outcrop hydrothermal circulation, *Nat. Commun.*, *6*, 7567, doi:10.1038/ncomms8567.

Winslow, D. M., A. T. Fisher, and K. Becker (2013), Characterizing borehole fluid flow and formation permeability in the ocean crust using linked analytic models and Markov chain Monte Carlo analysis: Borehole flow and formation permeability, *Geochem. Geophys. Geosyst.*, *14*, 3857–3874, doi:10.1002/ggge.20241.

Zyvoloski, G. A., B. A. Robinson, Z. V. Dash, S. Kelkar, H. S. Viswanathan, R. J. Pawar, and P. H. Stauffer (2011), Software users manual (UM) for the FEHM application version 3.1, *Los Alamos Natl. Lab.*, 265.